ORIGINAL PAPER

# Electrodeposition and characterization of zinc–nickel–iron alloy from sulfate bath: influence of plating bath temperature

M. M. Abou-Krisha · F. H. Assaf · S. A. El-Naby

**Abstract** The electrodeposition of ternary zinc–nickel–iron alloy was studied in acidic sulfate bath. The comparison between Zn, Ni, and Fe deposition and Zn–Ni and Zn–Ni–Fe co-deposition revealed that the remarkable inhibition of Ni and Fe deposition takes place due to the presence of $Zn^{2+}$ in the plating bath. The increase in corrosion resistance of ternary deposits is not only attributed to the formation of $\gamma$-$Ni_2Zn_{11}$ phase but also to iron co-deposition and formation of iron phase. It was also found that the bath temperature has a great effect on the surface appearance and the deposit composition. The investigation was carried out using cyclic voltammetry and galvanostatic techniques for electrodeposition, while linear polarization resistance and anodic linear sweeping voltammetry techniques were used for corrosion study. Morphology and chemical composition of the deposits were characterized by means of scanning electron microscopy and atomic absorption spectroscopy.

**Keywords** Electrodeposition · Phase structure · Surface morphology · Corrosion resistance · Ternary Zn–Ni–Fe alloy

## Introduction

Many efforts have been made to develop brightly corrosion resistant steel sheets especially for automotive body panels. Recently, it has been shown that electrodeposited zinc–iron group metal alloys are suitable materials for this application [1]. Zinc–nickel alloy coatings are being extensively studied instead of cadmium coating due to their good corrosion protection property [2], superior formability, and improved welding characteristics [3–5]. Zn–Ni alloys containing 15–20 wt.% nickel were shown to possess four times more corrosion resistance than cadmium–titanium deposit [6]. The Zn–Fe alloy is widely used in electroplating procedures due to its low cost. It is well known that Zn–Ni and Zn–Fe alloys are good substitute for cadmium, which has two environmental hazards (cadmium and cyanide). It was observed that the addition of Fe to Zn–Ni alloy has led to the formations of ternary Zn–Ni–Fe alloys, which improve the appearance of the alloy and increase its corrosion resistance [7]. Zn–Ni–Fe alloys are valuable for their leveling action [8] and are used also as a source in hydrogen evolution reaction [9].

The electrodeposition of Zn with Fe group metals was classified as anomalous, i.e., the less noble Zn deposits preferentially in most plating conditions. Although this phenomenon has been known since the beginning of the twentieth century, the mechanism still needs further elucidation. Among the hypotheses found in literature which explain this anomaly [10–14] is the so-called 'hydroxide suppression mechanism' [12–14]. This model, initially proposed by Dahms and Croll [12] for the Fe–Ni system, suggests that the precipitation of a less noble metal hydroxide at the cathode is able to inhibit the deposition of the more noble metal. This metal hydroxide is believed to be formed due to a local pH increase. Based on this theory, deposition conditions that can cause surface pH increase would enhance the anomalous co-deposition [15–17]. Some recent studies on Zn/Fe group alloy [18–20] are in agreement with these ideas. Fabri Miranda et al. [19] verified again that the deposition of Ni is activated with an increase in solution pH of the Zn–Ni system in sulfate medium. Another aspect that plays an important role on the

M. M. Abou-Krisha (✉) · F. H. Assaf · S. A. El-Naby
Faculty of Science, Chemistry Department,
South Valley University,
Qena 83523, Egypt
e-mail: m_abou_krisha@yahoo.com

Zn/Fe group anomalous co-deposition is the type of anion present in solution.

Another theory considers that the anomalous co-deposition process is associated with the underpotential deposition (upd) of the less noble metal [11, 20, 21]. It is well known that Zn upd occurs only in the presence of Fe group metals and is not observed in other Zn co-deposition process. Nevertheless, the Zn upd mechanism is still unclear. Besides, this approach hardly explains, for example, how high Zn contents in thick ZnNi alloy deposits can be generated by the upd of Zn monolayers. On the other hand, one can admit that both Zn hydroxide precipitation and Zn upd could take place at the electrode surface during ZnNi co-deposition. However, these two phenomena are not sufficient to account for the entire anomalous co-deposition process [19].

Two other papers on Ni–Fe electrodeposition propose different mechanisms. The mechanism of Lieder and Biallozor [22] assumes that $Ni^{2+}$ discharges first to form a thin layer which chemisorbs water to form adsorbed Ni $(OH)^+$; competition between the $Ni^{2+}$ and $Fe^{2+}$ to occupy active sites leads to the preferential deposition of Fe. Matlosz [23] has used a two-step reaction mechanism involving adsorbed monovalent intermediate ions for both electrodeposition of iron and nickel, as single metals, and combines them to develop a model for co-deposition. Anomalous effects are assumed to be caused by preferential surface coverage due to differences in Tafel rate constants for electrodeposition.

Wu et al. [24] have studied the effect of temperature on zinc–nickel co-deposition in chloride baths. They found that the polarization curves for zinc–nickel co-deposition were shifted towards less negative potentials and the percentage of deposited nickel increases with increasing temperature of the bath solution. Such behavior is primarily the result of intrinsically slow nickel kinetics.

The objective of the present work was to investigate the electrodeposition of Zn–Ni–Fe alloy in sulfate bath which was studied in fewer articles. The alloy composition and the morphology of the deposit were also studied under different plating bath temperatures. The results of the experimental approach are based essentially on the analysis of the cyclic voltammograms and galvanostatic measurements during the electroplating and linear polarization and anodic linear sweeping voltammetry for corrosion study.

## Experimental

The standard bath compositions for Zn–Ni–Fe deposits are given in Table 1. The electrolytes used for electrodeposition of Zn–Ni–Fe alloys were freshly prepared using Analar grade chemicals without further purification and were dissolved in appropriate amount of doubly distilled water.

The electrolytic cell used in the present work was discussed in detail in [25].

The electrodeposition process was usually performed on pure steel rod of cross-sectional area (0.196 $cm^2$) at pH=2.5 and current density 5.0 mA $cm^{-2}$ for 10 min at 30.0 °C. While investigating the influence of temperature, the electroplating was carried out at different temperatures. The reference electrode (a saturated Ag/AgCl/KCl) was mounted in a Luggin capillary, and a Pt sheet (6.0 $cm^2$) has been used as a counter electrode.

For electrochemical methods (cyclic voltammetric behavior, galvanostatic, measurements, linear polarization resistance, and anodic sweeping voltammetry techniques) EG&G Potentiostat/Galvanostat Model 273A controlled by a PC using 352 corrosion software was used. The influence of the examined conditions on the E-t and i-E profile was studied.

All cyclic voltammetry experiments were initiated at 0.0 V in a negative direction and reversed at −1.2 V in a positive direction to 0.0 V at a scan rate of 5 mV $s^{-1}$.

The surface morphology of the deposit was evaluated by a scanning electron microscope (SEM; JSM-5500 LV, SEM, JEOL, Japan). X-ray diffractometry (XRD) X'Pert Pro PANalytical was used to identify the phases of Zn–Ni–Fe alloys deposited. In order to determine the percentage composition of deposit [25], the deposit was stripped in 30% (v/v) HCl solution, diluted with doubly distilled water up to 100 $cm^3$, and analyzed to ascertain the Zn, Ni, and Fe contents in the deposited alloy using atomic absorption spectroscopy (Variian SpectrAA 55). Steel and copper sheets cathodes, of width 1.0 cm and 1.0 cm in length, were used for XRD analysis and for morphological properties (SEM) and chemical analysis, respectively. Steel and copper sheets are provided with a narrow strip of about 1-$cm^2$ area to which clamp terminals were attached for electrical contact.

The thicknesses were calculated as discussed else where in [25]. The values of electrochemical corrosion measurements of the coatings, $E_{corr.}$, the corrosion potential, $R_p$, the polarization resistance, $I_{corr.}$, the corrosion current, and corrosion rate were obtained and are given in Table 2.

Table 1 Basic electrolyte composition for the electrodeposition ternary Zn–Ni–Fe alloy

| Electrolyte composition | Concentration (M) |
| --- | --- |
| Zinc sulfate | 0.1 |
| Nickel sulfate | 0.1 |
| Ferrous sulfate | 0.1 |
| Sodium sulfate | 0.2 |
| Boric acid | 0.2 |
| Sulfuric acid | 0.01 |

**Table 2** Values of Zn, Ni and Fe amount in the deposit, total mass of the deposit (%, Zn, Ni, and Fe content), current efficiencies (%, Zn, Ni, Fe, and Zn–Ni–Fe deposits), thickness and electrochemical corrosion measurements of the deposit on copper sheet (2 cm$^2$) deposited galvanostatically from a bath containing 0.10 M ZnSO$_4$, 0.10 M FeSO$_4$, 0.10 M NiSO$_4$, 0.01 M H$_2$SO$_4$, 0.20 M Na$_2$SO$_4$, and 0.20 M H$_3$BO$_3$ at 5 mA cm$^{-2}$ for 10 min at different temperature

| Parameter | Temperature (°C) | | | |
|---|---|---|---|---|
| | 20 | 30 | 40 | 50 |
| Zn amount in the deposit (10$^{-5}$ g) | 141 | 126 | 90 | 75 |
| Ni amount in the deposit (10$^{-5}$ g) | 9.8 | 16.5 | 24.4 | 34 |
| Fe amount in the deposit (10$^{-5}$ g) | 1.6 | 2.4 | 2.6 | 3 |
| Total mass of the deposit (10$^{-5}$ g) | 152.4 | 144.9 | 117 | 112 |
| Zn content (%) | 92.5 | 86.9 | 77.1 | 66.9 |
| Ni content (%) | 6.4 | 11.4 | 20.6 | 30.3 |
| Fe content (%) | 1.1 | 1.7 | 2.3 | 2.8 |
| Zn–Ni–Fe deposit current efficiency ($e_{Zn–Ni–Fe}$, %) | 75.7 | 72.6 | 58.8 | 57.3 |
| $I_{corr.}$ (A cm$^{-2}$×10$^{-4}$) | 2.018 | 1.67 | 0.787 | 0.392 |
| $E_{corr.}$ (mV) | −648 | −608 | −589 | −561 |
| $R_p$ (k Ω) | 0.152 | 0.194 | 0.20 | 0.23 |
| Corrosion rate (milli-inch per year) | 30.4 | 22.21 | 17.14 | 8.32 |
| Thickness of the deposit (μm) | 1.05 | 1 | 0.8 | 0.7 |

## Results and discussion

### Electrochemical characterization of the deposited Zn, Ni, Fe, Zn–Ni, and Zn–Ni–Fe deposits

The electrodeposition of each Zn, Ni, and Fe alone and Zn–Ni or Zn–Ni–Fe together over the steel rod in bath solution at 30.0 °C was studied by cyclic voltammetry (Fig. 1). In the negative scan, the deposition of Zn alone started at about −1,110 mV which takes the same shape and is close to the potential of Zn–Ni and Zn–Ni–Fe co-deposition (at about −1,050 and −1,038 mV, respectively). It is clear that the deposition potential is shifted positively in the presence of Ni and Fe. This means that the corrosion resistance of Zn–Ni–Fe alloy is higher compared with the Zn–Ni alloy. Figure 1 shows also that the deposition of Ni alone and Fe alone start at about −900 and −960 mV, respectively; the growth of deposited layer increases gradually when the potential is shifted to more negative values. Although the polarization curve of Zn–Ni and Zn–Ni–Fe alloy deposition lie between the polarization curves of each deposition Zn and Ni and/or Fe, Zn–Ni–Fe alloy deposition potential is more noble than Zn–Ni deposition potential. This may be

due to co-deposition of iron into the alloy. This position suggested that the co-deposition enables Zn to deposit at more positive potential (i.e., shifts the deposition potential of Zn to less negative values) due to the presence of Ni$^{2+}$ and Fe$^{2+}$, which facilitates Zn deposition. However, the co-deposition of Ni and Fe shifted negatively in the presence of Zn$^{2+}$, which reduces Ni and Fe deposition. The cathodic peak which is started at about −577 mV may be attributed to the hydrogen evolution as reported before [25].

It is clear from the anodic part in the cyclic voltammograms (Fig. 1) that there is only one anodic peak at about −900 mV, which is attributed to the anodic dissolution of Zn deposited alone in the absence of Ni and Fe. There are also two anodic peaks at −100 and −540 mV that correspond to the dissolution of pure Ni and Fe, respectively, which deposited each alone. For Zn–Ni voltammogram, there are three peaks, as reported earlier [26], which correspond to the dissolution of the constituents of two
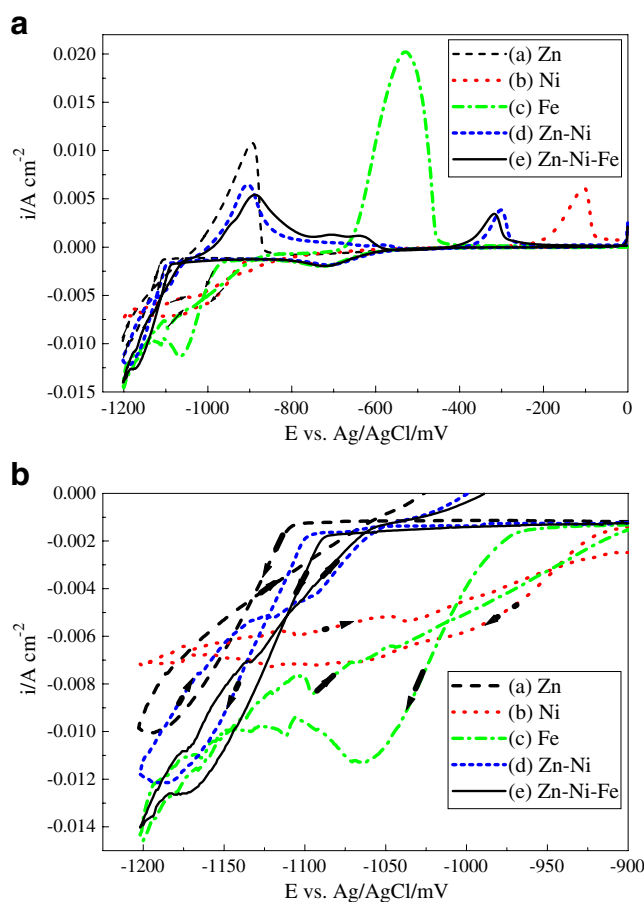


**Fig. 1** i-E curves (cyclic voltammograms) for steel in 0.10 M ZnSO$_4$ (**a**), 0.10 M NiSO$_4$ (**b**), 0.10 M FeSO$_4$ (**c**), 0.10 M ZnSO$_4$ and 0.10 M NiSO$_4$ (**d**), and 0.10 M ZnSO$_4$, 0.10 M NiSO$_4$, and 0.10 M FeSO$_4$ (**e**). The cathodic part of **a** is shown in **b** with 0.01 M H$_2$SO$_4$, 0.20 M Na$_2$SO$_4$, 0.20 M H$_3$BO$_3$ and scan rate 5 mV s$^{-1}$ at 30.0 °C

phases deposited, δ-phase ($Ni_3Zn_{22}$) and γ-phase ($Ni_5Zn_{21}$). The first and second anodic peaks correspond to the dissolution (de-alloying) of Zn from δ- and γ-phases, respectively, while the third peak corresponds to the dissolution of Ni. However, for Zn–Ni–Fe curve, there are four anodic peaks. The first dissolution anodic peak at −910 mV is attributed to the dissolution of zinc from pure Zn phase. The second anodic peak at about −741 mV that corresponds to dissolution of Zn from (γ-$Ni_2Zn_{11}$) phase. Therefore, the third and fourth anodic peaks at more noble potential, −678 and −384 mV, correspond to the dissolution of iron from iron–nickel phase and nickel from its phases, respectively.

The height of any peak gives an indication about the quantity of its phase in the deposit. Therefore, from Fig. 1, the increase in the height of the second peak and its shift to more noble direction reflects that the content of ($Ni_2Zn_{11}$) phase in the deposit increases for the deposition of Zn–Ni–Fe in comparison with Zn–Ni alloy deposition. The height of the third peak that corresponds to the dissolution of iron from its phase is too low compared with the height of that which corresponds to the dissolution of Fe which is deposited alone. In order to estimate the corrosion resistance of various coatings their corrosion potentials of Zn, Fe, Ni, Zn–Ni, and Zn–Ni–Fe were measured as −971, −334, −169, −980, and −608, respectively. These results revealed that the ternary Zn–Ni–Fe deposits exhibit higher corrosion resistance in comparison with Zn–Ni deposits. Furthermore, the results obtained agree with earlier investigations [7] of the electrodeposition of Zn–Ni–Fe alloys from chloride baths.

The results suggest the following sequence of events: first, $Ni^{2+}$ (or its monovalent intermediate) is adsorbed, followed by adsorption of $Fe^{2+}$ and then $Zn^{2+}$ (or their monovalent intermediate) onto the freshly adsorbed and deposited nickel. The adsorption of zinc ions inhibits subsequent deposition of nickel and iron, although it does not block it completely.

Effect of plating bath temperature

The temperature of the plating bath is an important variable in Zn–Ni–Fe alloy co-deposition. Table 2 shows a gradual decrease of both Zn content and cathodic current efficiency of Zn–Ni–Fe alloy deposition with increasing of the temperature. The decrease of both Zn content and cathodic efficiency of Zn–Ni–Fe alloy deposition with rise in temperature may be attributed to hydrogen evolution (which increases with temperature) on cathode surface on account of deposited metallic coating. Thus, the results are in accordance with the fact that the main effect of rising the temperature of the plating bath is, to some extent, to relieve the anomalous nature of the co-deposition with decreasing

the zinc content of the deposit. Figure 2 shows the cyclic voltammograms which indicate that the second and third peaks, which are overlapping at 40 °C and 50 °C, and the fourth peak is increased as the temperature is appreciably increased. This means that both nickel and iron content in alloy are increased with temperature (Table 2). The increase of nickel and iron content may be attributed to a decrease in the overpotential of nickel and iron at higher temperature. It is interesting to mention that the cathodic peak current which starts at −574 mV, which can probably be ascribed to the hydrogen evolution, occurred in the presence of $H_2SO_4$ [25] and increases with the temperature rise. In addition, there is a large increase in the cathodic deposition peak currents of the alloy with increasing the temperature. This is due to a parallel increase of cathodic charge with the decrease of nucleation overpotential. It is clear from the cyclic voltammetric curves that the increase of the bath temperature, from 20 °C to 50 °C, causes a decrease in the
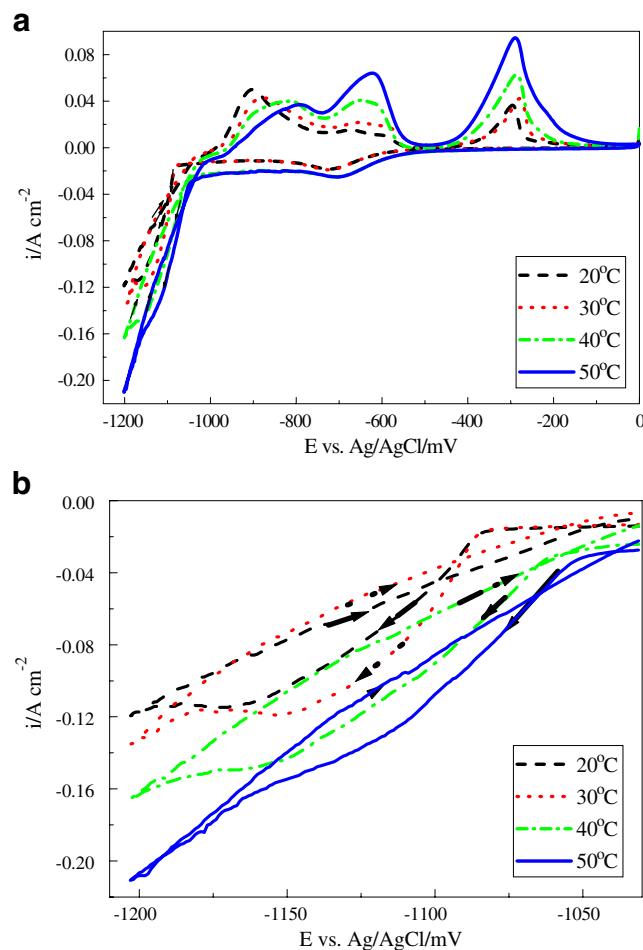


**Fig. 2** i-E curves (cyclic voltammograms) for steel in 0.10 M $ZnSO_4$, 0.10 M $FeSO_4$, 0.10 M $NiSO_4$, 0.01 M $H_2SO_4$, 0.20 M $Na_2SO_4$, and 0.20 M $H_3BO_3$ and scan rate 5 mV s$^{-1}$ at different temperatures. The cathodic part of **a** is shown in **b**

rate of zinc deposition, giving the observed decrease of the first dissolution peak (pure Zn phase). However, the second and third (overlapping) peaks are shifted to the positive side as a result of increasing iron and nickel content, leading to more improvement in the corrosion resistance of the deposit.

The galvanostatic measurements in Fig. (3) reveal that increasing the temperature of the plating bath decreases the cathodic deposition potential of the alloy. It is clear that the co-deposition proceeds at 50 °C needs low overpotential to create the initial nucleus, while at 20 °C, more overpotential is needed. This may be due to the fact that the content of both Ni and Fe, which needs low overpotential to create the initial nucleus, are increased with temperature rise.

Increasing the temperature from 20°°C to 50°°C activates nickel and iron deposition, thus producing a higher nickel and iron content in alloys at 50°°C. Such behavior is primarily the result of intrinsically slow nickel and iron kinetics. This may be ascribed to the re-dissolution of Zn deposited in the acidic medium and also to the increase of the diffusion process at elevated temperatures [27]. Since the rate of dissolution of Zn was much higher than that of Ni and Fe, it seemed that the Ni and Fe content in the alloy layer increased at these temperatures.

The phase structure was investigated in $Na_2SO_4$ solution containing complex forming ions in which a Zn–Ni–Fe alloy is completely dissolved. Namely, it is well known that pure Zn dissolves while zinc alloys do not dissolve in $Na_2SO_4$ solution, while in the presence of a small amount of a complex-forming agent (EDTA), both Zn and its alloys dissolve. Similar results for the dissolution of Zn–Ni alloy were obtained by Bates [28]. Figure 4 displays the anodic linear sweep voltammograms obtained during the dissolution of the deposit. The dissolution of Zn–Ni–Fe alloy takes place under three voltammetric peaks; hence, three phases
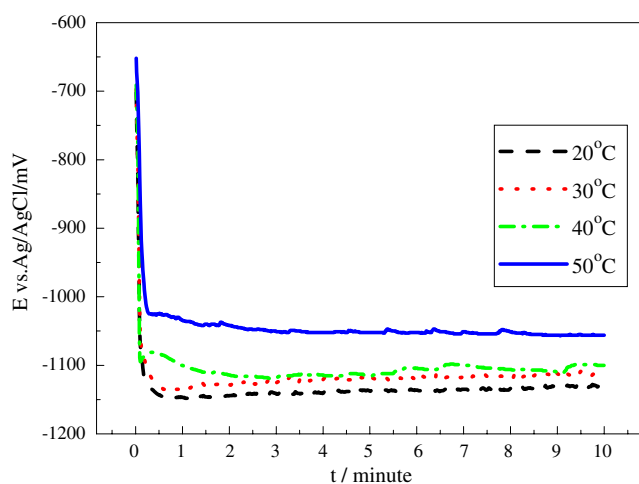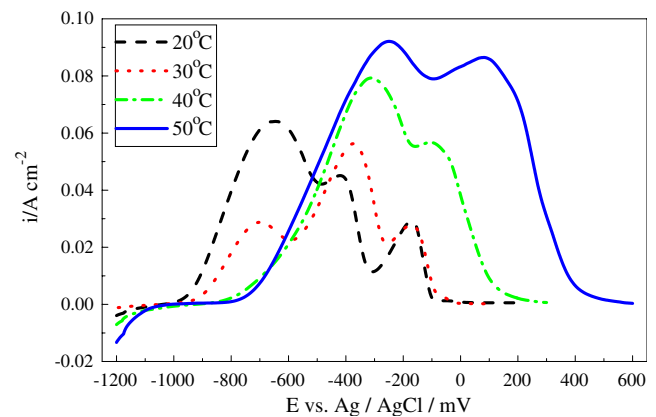


Fig. 4 ALSVs of Zn–Ni–Fe alloy electrodeposited on steel from a bath containing 0.10 M $ZnSO_4$, 0.10 M $NiSO_4$, 0.10 M $FeSO_4$, 0.01 M $H_2SO_4$, 0.20 M $Na_2SO_4$, 0.20 M $H_3BO_3$ at 5 mA cm$^{-2}$ for 10 min (at different temperatures) in 0.5 M $Na_2SO_4$ + 0.05 M EDTA solution at scan rate 5 mV s$^{-1}$ at 30 °C

were obtained. The anodic current peak at a potential of −625 mV corresponds to the dissolution of zinc from the first pure Zn phase. The second peak at −422 mV represents the dissolution of zinc from ($\gamma$-$Ni_2Zn_{11}$) phase which overlap with the dissolution of iron from its phase. The third anodic peak at more noble potential characterizes the dissolution of nickel from its phases. Figure 4 shows that at relatively low temperature, 20 °C, pure zinc is found with high amount but Ni-rich phases present in low percentage in the deposit. This is observed from the comparison between the heights of the peaks with each other. Rising of the temperature of the plating bath leads to more decrease in the height of the first dissolution peak, corresponding to a more decrease of pure Zn content in the deposit, which disappears at higher temperature, 40–50 °C. However, a more increase in the height of the second current peak is observed, leading to formation of more $\gamma$-$Ni_2Zn_{11}$ and iron phases. An increase in the oxidation of Ni from its phase can be understood from increasing of the height of the third current peak. The second and third anodic peaks were also shifted to more positive direction, indicating an increase in the content of the more noble component of the alloy (i.e., Ni and Fe).

Figure 5 represents the anodic linear polarization curves at different bath plating temperature. It is clear from this figure that the corrosion potential is shifted to more noble potential with the temperature rise. Thus, the improvement achieved in the corrosion resistance of deposits can be explained by the increase of nickel and iron content. Therefore, the temperature rise reduces the inhibiting effect of zinc on the nickel and iron electrodeposition.

Table 2 illustrates the dependence of Zn–Ni–Fe alloy composition on the plating bath temperature. It is noticeable that zinc content is negatively correlated with the rise in deposition temperature, while iron and nickel tend to



Fig. 3 E-t curves for steel in 0.10 M $ZnSO_4$, 0.10 M $FeSO_4$, 0.10 M $NiSO_4$, 0.01 M $H_2SO_4$, 0.20 M $Na_2SO_4$, and 0.20 M $H_3BO_3$ at 5 mA cm$^{-2}$ for 10 min at different temperatures
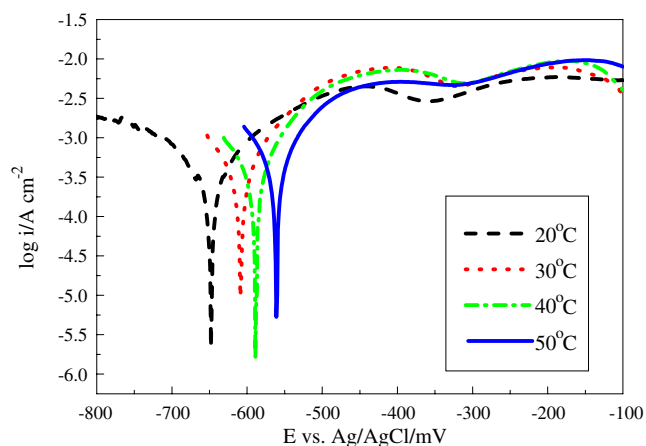
**Fig. 5** log i-E curves of Zn–Ni–Fe alloy electrodeposited on steel from a bath containing 0.10 M ZnSO$_4$, 0.10 M FeSO4, 0.10 M NiSO$_4$, 0.01 M H$_2$SO$_4$, 0.20 M Na$_2$SO$_4$ and 0.20 M H$_3$BO$_3$ at 5 mA cm$^{-2}$ for 10 min at different temperatures in 50 cm$^3$ 0.05 M HCl at 30 °C

increase, forming Fe- and Ni-rich alloys at higher temperatures. The increase of both nickel and iron may be attributed to the lower overpotential of nickel and iron deposition at higher temperatures. Increasing of the temperature enhances the concentration of metal ions in the cathodic diffusion zone because rates of diffusion and convection are increased with temperature. Under these conditions, nickel and iron deposited at the expense of zinc. This result reflects the greater effectiveness of diffusion over depolarization. It is clear that the cathodic current efficiency was slightly decreased with rising temperature; this may be attributed to hydrogen evolution or to a sharp decrease of zinc deposition efficiency. These results are in agreement with these reported by Ashassi-Sorkhabi et al. [29] for the electrodeposition of Zn–Ni in chloride bath. Results show that a decrease in the thickness of the deposited layer follows these changes, which is attributed to the decrease of zinc content in the alloy which possesses the lower density. It is clear from the measured electrochemical corrosion values, which are recorded in Table 2, that the corrosion potential and $I_{corr.}$ decrease with the increasing the temperature. It is clear that the polarization resistance of the deposit increased with increasing Ni and Fe content in the alloy, but the corrosion rate was decreased.

Corresponding changes in the structure and morphology can be observed from the SEM analysis that depends strongly on the temperature of the electrolytic bath. Figure 6a,b shows the influence of the deposition temperature on Zn–Ni–Fe deposits morphology. It can be seen that deposits obtained at low deposition temperature (Fig. 6a) show a low compact and non-homogeneous structure; this may be due to the high content of zinc with respect to nickel and iron. On the other hand, with increasing the deposition temperature, the compactness of Zn–Ni–Fe

deposits increase and the grain size was reduced due to an improvement in the nucleation rate (Fig. 6b).

## Conclusion

The obtained results revealed that:

- The ternary Zn–Ni–Fe deposits exhibit higher corrosion resistance in comparison with Zn–Ni deposits.
- The increase in corrosion resistance of ternary deposits is not only attributed to formation of ($\gamma$-Ni$_2$Zn$_{11}$) phase but also to iron co-deposition.
- The temperature has a great influence on the Zn–Ni–Fe deposition since nickel and iron content increased as the temperature increased.
- With increasing of the deposition temperature, the compactness of Zn–Ni–Fe deposits increases and the
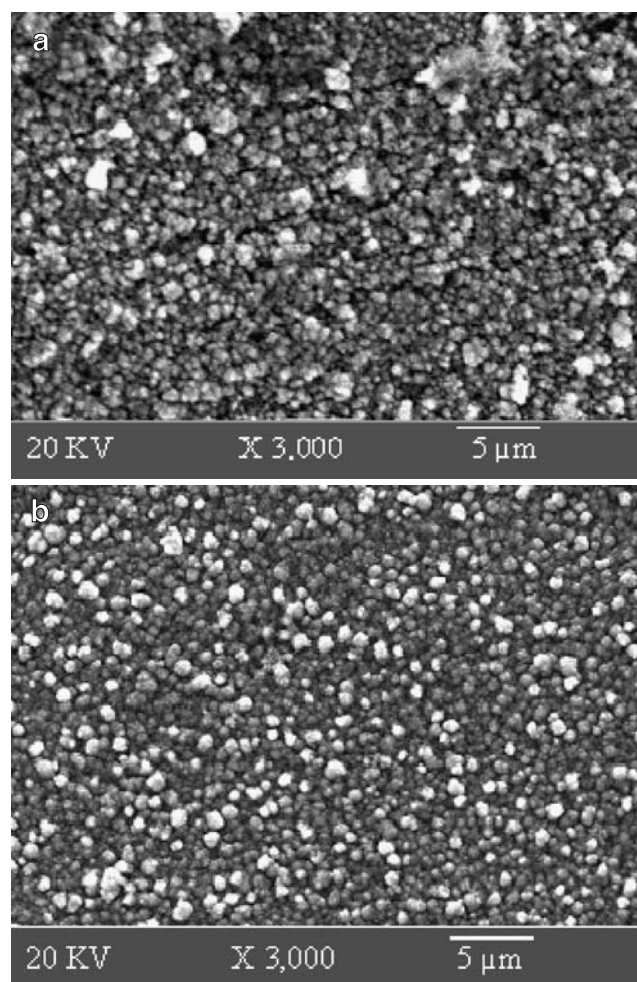


**Fig. 6** SEM photograph of electrodeposited Zn–Ni–Fe alloy on steel from a bath containing 0.10 M ZnSO$_4$, 0.10 M NiSO$_4$, 0.10 M FeSO$_4$, 0.01 M H$_2$SO$_4$, 0.20 M Na$_2$SO$_4$, 0.20 M H$_3$BO$_3$ at 5 mA cm$^{-2}$ for 10 min at 20.0 °C (**a**) and 50.0 °C (**b**)

grain size was reduced due to an improvement in the nucleation rate, which also indicates low zinc content.

# References

1. Zhang Z, Leng WH, Shao HB, Zhanga JQ, Wang JM, Cao CN (2001) J Electroanal Chem 516:130 doi:10.1016/S0022-0728(01)00665-9
2. Hsu GF (1984) Plat Surf Finish 71:52
3. Lin YP, Selman JR (1993) J Electrochem Soc 140:1299 doi:10.1149/1.2220974
4. Miyoshi Y (1991) J ISIJ Int 31:1 doi:10.2355/isijinternational.31.1
5. Yau YH, Fountolakis SG (1990) Minerals, Metals and Materials Society, p 143
6. Safranek WH (ed) (1986) The properties of electrodeposited metal and alloy. AESF, Orlando, FL, p 466
7. Younan MM, Oki T (1996) J Appl Electrochem 26:537 doi:10.1007/BF01021978
8. Safranck WH (1957) German Patent No. 1016527
9. Ananth MV, Parthasaradhy NV (1997) Int J Hydrogen Energy 22:747 doi:10.1016/S0360-3199(96)00206-6
10. Brenner A (1963) Electrodeposition of alloys, vol. 2. Academic, New York, p 194
11. Nicol MJ, Philip HI (1976) J Electroanal Chem 70:233 doi:10.1016/S0022-0728(76)80109-X
12. Dahms H, Croll IM (1965) J Electrochem Soc 112:771 doi:10.1149/1.2423692
13. Fukushima H, Akiyama T, Yano M, Ishikawa T, Kammel R (1993) J ISIJ Int 33:1009 doi:10.2355/isijinternational.33.1009
14. Akiyama T, Fukushima H (1992) J ISIJ Int 32:787 doi:10.2355/isijinternational.32.787
15. Fukushima H, Ahiyama T, Higishi K, Kammel R, Karimkhani M (1990) Metall 44:754
16. Yan H, Dawns J, Boden PJ, Harris SJ (1996) J Electrochem Soc 143:1577 doi:10.1149/1.1836682
17. Liao Y, Gabe DR, Wilcox GD (1998) Plat Surf Finish 85:60
18. Tsuru T, Kobayashi S, Akyama T, Fukushima H, Gogia SK, Kammel R (1997) J Appl Electrochem 27:209 doi:10.1023/A:1018460109175
19. Fabri Miranda FJ, Barcia OE, Mattos OR, Wiart R (1997) J Electrochem Soc 144:3441 doi:10.1149/1.1838030
20. Fratesi R, Roventi G, Giuliani G, Tomachuk CR (1997) J Appl Electrochem 27:1088 doi:10.1023/A:1018494828198
21. Swathirajan S (1987) J Electroanal Chem 221:211 doi:10.1016/0022-0728(87)80258-9
22. Lieder M, Biallozor S (1998) Surf Coat Technol 26:23
23. Matlosz M (1993) J Electrochem Soc 140:2272 doi:10.1149/1.2220807
24. Wu Z, Fedrizzi L, Bonora PL (1996) Surf Coat Technol 85:170 doi:10.1016/0257-8972(96)02857-5
25. Abou-Krisha MM (2005) J Appl Surf Sci 252:1035 doi:10.1016/j.apsusc.2005.01.161
26. Abou-Krisha MM, Assaf FH, Toghan AA (2007) J Solid State Electrochem 11:244 doi:10.1007/s10008-006-0099-x
27. Lee HY, Kim SG (2000) Surf Coat Technol 135:69 doi:10.1016/S0257-8972(00)00731-3
28. Bates JA (1994) Plat Surf Finish 81:36
29. Ashassi-Sorkhabi H, Hagrah A, Parvini-Ahmadi N, Manzoori (2001) J Surf Coat Technol 140:278 doi:10.1016/S0257-8972(01)01032-5